# Normal Modes in Ferromagnetic Nanoparticles: A Dynamical Matrix Approach

M. Grimsditch*
*Materials Science Division, Argonne National Laboratory, Argonne, IL 60439*

L. Giovannini, F. Montoncello and F. Nizzoli
*Dipartimento di Fisica, Università di Ferrara and Istituto Nazionale per la Fisica della Materia, Via del Paradiso 12, I-44100 Ferrara, Italy*

Gary K. Leaf† and Hans G. Kaper‡
*Mathematics and Computer Science Division, Argonne National Laboratory, Argonne, IL 60439*

We present a method to compute the magnetic normal modes of a ferromagnetic particle. The method is a hybrid of micromagnetic simulations and a "dynamical matrix" approach similar to that used for vibrational studies. We use the method to calculate the normal modes of an Fe parallelepiped and compare the results with the modes recently extracted from a purely micromagnetic simulation. The results of the two approaches are in excellent agreement. We discuss the pros and cons of both approaches. We also present information on standing waves with wavevector perpendicuar to the applied field and on a family of modes localized at the particle ends.

PACS numbers: 75.75.+a, 75.30.Ds
Keywords: Micromagnetics, spin excitations, normal modes, numerical simulations, dynamical matrix approach

## I. INTRODUCTION

The calculation of the magnetic normal modes of small particles is an extremely complicated problem when both dipolar and exchange contributions are taken into account. Walker[1,2] succeeded in obtaining solutions for a few relatively simple geometrical shapes by ignoring exchange contributions. Analytical approaches[3,4] have had some success but require certain assumptions regarding the mode profiles. Micromagnetic simulations[5] based on the Landau–Lifshitz–Gilbert equation have provided additional insight into some of the normal modes of small magnetic particles. Micromagnetic simulations typically rely on codes[6] designed for the calculation of the static ground state of a magnetic particle. With these codes, it is possible to track the time evolution of the average magnetization of a particle. Information about the normal modes is then extracted by means of the Fourier transform. However, only modes with nonzero average magnetization can be observed, and the codes in their present form yield no information about the profiles (frequencies and eigenvectors) of the normal modes. Only recently has the micromagnetic approach been extended to enable the study of profiles of standing magnetic waves in small disks for the special case of an oscillatory in-plane applied field.[7] In this case, only modes antisymmetric with respect to a plane perpendicular to the applied field were obtained. The so-called hybrid method[8] with a tridimensional mesh of tetrahedral elements has been used to compute demagnetizing fields, and a similar method with a bidimensional mesh of triangular elements has been used to compute various magnetic modes oscillating across a strip of infinite length.[9] An attempt to justify the presence in experimental spectra[10,11] of localized modes and of standing modes quantized in the direction of the applied field (similar to the backward volume waves in a film) and of its normal (Damon–Eshbach (DE)-like modes) has been presented recently in an approximate theoretical framework that includes the boundary conditions at the lateral element edges and the strong inhomogeneity of the internal magnetic field.[12,13] However, some simplifying assumptions on the mode profiles were also introduced.

By extending the simulation approach, using a code which independently tracks the time evolution of all the "spins" in a particle, the authors of the present paper showed recently[14] that it is possible to reconstruct normal modes from the Fourier transforms of each individual spin. To demonstrate the effectiveness of the technique, we computed the normal modes of a polycrystalline iron particle in the form of a rectangular parallelepiped measuring $116 \times 60 \times 20$ nm and magnetized along the long axis. Good agreement was obtained when mode frequencies were compared to those predicted by existing standing-wave approximations. However, the actual mode profiles were considerably more complex than those predicted by standing-wave theory, and localized modes—absent in standing-wave theory—were also found to be present.

In a micromagnetic simulation, the sample is divided into cells, the magnetization is assumed uniform in each cell and to precess about its equilibrium direction under the influence of the external field and the dipolar and exchange forces due to all the spins in the system. Given the similarity between this and conventional molecular dynamics,

where each atom obeys Newton's laws in the potential of the surrounding atoms, it seems reasonable to solve the normal-mode problem in a manner similar to the dynamical matrix approach used for atomic vibrations. A similar approach has been used[15,16] in the case of magnetic multilayers, where the in-plane translational symmetry reduces the number of independent variables of the dynamical problem to twice the number of the layers. In the present article we present the results of such a "dynamical matrix" approach for magnetic normal modes of nanometric small particles which, with respect to multilayers, are laterally confined and require a subdivision of the particle in a large number of cells. The method presents several advantages. (i) A single calculation yields the dynamical magnetization profiles (frequencies and eigenvectors) of all the modes of any symmetry; (ii) Particles of any shape can be considered, at least in principle; (iii) No a priori limitation is imposed on the form and pinning of the modes; and (iv) The computation time is affordable.

In Sec. II we outline the theoretical approach. In Sec. III we apply the formalism to the exact same particle as investigated in Ref. 14 to assess the mathematical viability of the dynamical matrix approach.

## II. THEORY

As a starting point we recall that a single film, uniformly magnetized, can be treated in terms of the motion of a single dipole. The dynamical matrix is obtained by writing the total energy as a function of the orientation of the dipole in terms of the polar angles $\phi$ and $\theta$; the torque is then obtained from the second derivative of the energy with respect to the polar angles. The precession frequency is given by the determinant equation[17]

$$\begin{vmatrix} \dfrac{E_{\phi\phi}}{\sin\theta} & \dfrac{E_{\phi\theta}}{\sin\theta} - \dfrac{iM_s\Omega}{\gamma} \\ \dfrac{E_{\theta\phi}}{\sin\theta} + \dfrac{iM_s\Omega}{\gamma} & \dfrac{E_{\theta\theta}}{\sin\theta} \end{vmatrix} = 0. \tag{1}$$

Here, $E_{\alpha\beta}$ is the second derivative of the total energy with respect to the polar angles $\alpha$ and $\beta$; $\Omega$ is the frequency, $M_s$ the saturation magnetization, and $\gamma$ the gyromagnetic ratio. This method can be generalized to the case of a particle divided into $N$ cells—rectangular parallelepipeds—with a square base of size $d$ and height $h$; $h$ can be identified with the thickness of the particle.

We consider a reference frame with the $z$-axis along the normal to the particle, the $x$ and $y$-axes along the particle sides. Let the polar angles that define the orientation of magnetization in the $n$th cell be $\phi_n$ and $\theta_n$, so that the (unitary) vector specifying the magnetization direction is given in Cartesian coordinates by

$$\boldsymbol{m}_n = (\sin\theta_n\cos\phi_n, \sin\theta_n\sin\phi_n, \cos\theta_n). \tag{2}$$

With this choice, $\theta_n$ is the angle between the magnetization and the $z$-axis, $\phi_n$ the in-plane angle with the $x$-axis. The energy density $E$ must then be written as a function of these angles and the material parameters.

As shown in Appendix A, the equations leading to the determinant condition (1) can be generalized giving rise to the system of $2N$ homogeneous linear equations,

$$\begin{cases} \displaystyle\sum_{j=1}^{N}\left(-\frac{E_{\theta_k\phi_j}}{\sin\theta_k}\right)\delta\phi_j + \sum_{j=1}^{N}\left(-\frac{E_{\theta_k\theta_j}}{\sin\theta_k}\right)\delta\theta_j - \lambda\,\delta\phi_k = 0, \quad k = 1,\ldots,N, \\ \displaystyle\sum_{j=1}^{N}\frac{E_{\phi_k\phi_j}}{\sin\theta_k}\,\delta\phi_j + \sum_{j=1}^{N}\frac{E_{\phi_k\theta_j}}{\sin\theta_k}\,\delta\theta_j - \lambda\,\delta\theta_k = 0, \quad k = 1,\ldots,N, \end{cases} \tag{3}$$

where $\lambda = iM_s\Omega/\gamma$, and $\delta\theta_j$ and $\delta\phi_j$ are the small angles that define the deviations of the magnetization in each cell with respect to the ground state. By suitable exchanges of rows (or columns) the system of Eqs. (3) can be transformed in an eigenvalue problem,

$$B\boldsymbol{v} = \lambda\boldsymbol{v}$$

where $\boldsymbol{v} = (\delta\phi_1, \delta\theta_1, \ldots, \delta\phi_N, \delta\theta_N)$ and the matrix elements are given by

$$\begin{aligned} B_{2k-1,2j-1} &= -\frac{E_{\theta_k\phi_j}}{\sin\theta_k}, \quad & B_{2k-1,2j} &= -\frac{E_{\theta_k\theta_j}}{\sin\theta_k}, \\ B_{2k,2j-1} &= \frac{E_{\phi_k\phi_j}}{\sin\theta_k}, \quad & B_{2k,2j} &= \frac{E_{\phi_k\theta_j}}{\sin\theta_k}, \end{aligned} \tag{4}$$

for $k, j = 1, \ldots, N$. The expressions of these matrix elements depend on the choice of the dynamical variables. Instead of $\delta\theta$ and $\delta\phi$, one could use the polar components $\delta m_\theta = M_s\,\delta\theta$ and $\delta m_\phi = M_s \sin\theta\,\delta\phi$ (Ref. 18).

When the cells are decoupled, the dynamical matrix (4) is block-diagonal and consists of $N$ $2 \times 2$ submatrices. When the cells are coupled, as is generally the case, it is necessary to include the off-diagonal coupling submatrices with $k \neq j$.

Once the eigenvectors $\boldsymbol{v}$ are obtained, the dynamical magnetization $\delta\boldsymbol{m}$ in Cartesian coordinates and in units of $M_s$ is given by

$$\delta\boldsymbol{m}_k = (-\sin\theta_k \sin\phi_k\,\delta\phi_k + \cos\theta_k \cos\phi_k\,\delta\theta_k, \sin\theta_k \cos\phi_k\,\delta\phi_k + \cos\theta_k \sin\phi_k\,\delta\theta_k, -\sin\theta_k\,\delta\theta_k).$$

Although the collection of all $\delta\boldsymbol{m}_k$ defines the mode profile, it must be remarked that $\delta\boldsymbol{m}_k$ is a complex vector, because $\delta\phi_k$ and $\delta\theta_k$ are, in general, complex. A particularly interesting common case corresponds to an in-plane magnetized particle, where $\cos\theta_k = 0$ and $\sin\theta_k = 1$; in this case, it can be shown that the solution has the form $\boldsymbol{v} = (i\widehat{\delta\phi}_1, \delta\theta_1, i\widehat{\delta\phi}_2, \delta\theta_2, \ldots)$, where the amplitudes $\widehat{\delta\phi}_k$ and $\delta\theta_k$ are real. In other words, the $z$-components of $\delta\boldsymbol{m}_k$ are out of phase with the in-plane ($x$ and $y$) components.

The energy density can be written as a sum of Zeeman $E_z$, exchange $E_{\text{exc}}$, and dipolar $E_{\text{dip}}$ energies. The first two terms are straightforward and are equivalent to what is used in micromagnetic simulations, namely

$$E_z = -M_s \boldsymbol{H} \cdot \sum_{j=1}^{N} \boldsymbol{m}_j, \tag{5}$$

where $\boldsymbol{H}$ is the external field. For the exchange, we have the expression

$$E_{\text{exc}} = \frac{A}{d^2} \sum_{j=1}^{N} \sum_{n} (1 - \boldsymbol{m}_j \cdot \boldsymbol{m}_n), \tag{6}$$

where the second sum extends over the nearest neighbors of cell $j$, $A$ is the exchange coupling constant, and the effective exchange strength scales as $d^{-2}$.

The dipolar energy is by far the most difficult to treat. In the simulations reported in Ref. 14, the dipolar field was obtained from a complete solution of the Poisson equation at every step.[8] Such an approach is not well suited to yield the derivatives needed for the torque matrix. An alternative approach, also often adopted in micromagnetics, is to write the dipolar energy as a sum of the interactions between the magnetic moments $\boldsymbol{m}_k$ representative of the magnetization in each cell, by means of a demagnetizing tensor $\overleftrightarrow{N}(k,j)$[19,20],

$$E_{\text{dip}} = \frac{M_s^2}{2} \sum_{k=1}^{N} \sum_{j=1}^{N} \boldsymbol{m}_k \cdot \overleftrightarrow{N}(k,j) \boldsymbol{m}_j. \tag{7}$$

The problem thus reduces to the calculation of the tensor elements $\overleftrightarrow{N}(k,j)$. It should be noted that the latter expression is particularly useful within our approach, because the derivative of the energy applies only to the moments $\boldsymbol{m}_k$. (The demagnetizing tensor depends exclusively on the geometry and discretization of the magnetic particle.) In this framework it is implicitly assumed that the demagnetizing field is constant in each cell and equal to its average value.

We adopted two approaches, labeled Method A and Method B, to evaluate $\overleftrightarrow{N}(k,j)$. Method A evaluates the interactions of the magnetic surface charges from every cell (produced by the uniform magnetization inside each cell). Explicit expressions for $\overleftrightarrow{N}$ are given in Ref. 19. The same approach is used by default in the OOMMF code.[6] Method B, also used in micromagnetic simulations, assumes that the $\overleftrightarrow{N}(k,j)$ are given by point-dipole interactions, with the dipoles at the center of each (in this case) cubic cell.[21] The elemental parallelepiped is obtained as a stack along the normal to the particle of a proper number $N_z$ of cubic cells, such that $dN_z = h$. This approach implies that the sums over the in-plane cells in the expressions (5)–(7) are accompanied by a sum over the $N_z$ cubic cells along the $z$-axis. To have a constant magnetization in each parallelepiped, one must also assume that the moments $\boldsymbol{m}_k$ do not depend on $z$. It is known that the point-dipole approximation produces small errors, especially for neighboring cells.[20]

Explicit expressions for the second derivatives of the energy are given in Appendix B. We will use both Method A and Method B to compute the dipolar energy and to evaluate the normal mode frequencies and compare the results with the full calculation in Ref. 14.

TABLE I: Frequencies, in GHz, of normal modes of a $116 \times 20 \times 60$ nm Fe particle with a field of 10 kOe applied along the long axis. The symmetric and antisymmetric end modes are essentially degenerate at this field. The modes labeled as "$n$-nodes" correspond to the standing wave-like modes, with wavevectors along the field direction, reported in Ref. 14.

| Method | Cell size | Mode | | | | |
|---|---|---|---|---|---|---|
| (number of cells) | (nm) | Fundamental | End mode | 6-nodes | 10-nodes | $9 \times 2$-nodes |
| Ref. 14 ($29 \times 15 \times 5$) | $4 \times 4 \times 4$ | 52.9 | 30.2 | 56.6 | 89.3 | 94.4 |
| A ($29 \times 15 \times 1$) | $4 \times 4 \times 20$ | 53.1 | 30.0 | 55.5 | 86.5 | 91.7 |
| A ($58 \times 30 \times 1$) | $2 \times 2 \times 20$ | 52.4 | 29.3 | 55.5 | 90.4 | 94.2 |
| B ($29 \times 15 \times 5$) | $4 \times 4 \times 4$ | 52.9 | 28.3 | 54.8 | 85.2 | 90.7 |
| B ($58 \times 30 \times 10$) | $2 \times 2 \times 2$ | 52.7 | 28.8 | 55.6 | 90.3 | 94.3 |
| OOMMF ($29 \times 15 \times 1$) | $4 \times 4 \times 20$ | 52.6 | 29.5 | 55.1 | — | — |

## III. THE NORMAL MODES OF AN Fe BRICK-SHAPED PARTICLE

For systems with a small number of cells (typically less then 100), the system of Eqs. (3) can be solved directly with symbolic mathematics software. The second derivatives need not to be evaluated analytically, and the solutions of the determinant equation can be obtained with a few lines of code. However, to be able to treat realistic cases, it was necessary to develop a computer code based on the analytical formulas of the previous section. With this code, we are able to treat particles with up to 1800–2000 cells with computation times less than one hour on a standard PC.

We have computed the magnetic excitations of a $116 \times 60 \times 20$ nm Fe particle in an externally applied field of 10 KOe along the $x$-axis (116 nm), neglecting anisotropy and using the same parameters as in Ref. 14. The ground state calculated with the OOMMF code was used as a starting point for the dynamical calculations; the magnetization was in-plane. Cells with $d = 4$ and $d = 2$ nm yield 435 and 1740 eigenfrequencies, respectively. To make a comparison with the results in Ref. 14, it is necessary to select the same modes discussed in that article, either by plotting the profiles of the modes in the frequency range of interest or on the basis of their symmetry. We found that the mode profiles obtained from the dynamical matrix approach were almost indistinguishable from those of the micromagnetic approach,[14] which involved the Fourier transform of the time evolution of the magnetization. With this in mind we restrict our comparison to the frequencies of the individual modes. Table I gives a comparison of the frequencies of various modes found in Ref. 14 and those calculated with our two approximations for the dipolar field. We also investigate the effect of changing the number of computational cells in the particle.

Included in Table I are the frequencies extracted by performing a Fourier transform on the time dependence of the average magnetization obtained using OOMMF. The assignment of the modes in this case is made by noting that this approach only detects modes with $\langle \delta \boldsymbol{m}_i \rangle \neq 0$. In decreasing order of $\langle \delta \boldsymbol{m}_i \rangle$, these are the fundamental, the symmetric end mode, and the lowest order symmetric standing wave-like modes.

The modes of Table I are of three kinds: standing waves oscillating solely in the direction of the applied field (analogous of the backward modes in films), two-dimensional standing modes mixing oscillations in two perpendicular directions, and end modes evanescent in the direction of the applied field. Notice that the point-dipole Method B, although it considers a stack of cubic cells in the $z$ direction, actually assumes no dependence of the magnetization along $z$. In this sense it does not differ from Method A. We note that the calculations in Ref. 14 also did not observe any obvious $z$ dependence in the modes.

Overall it can be seen that the dynamical matrix approach yields results in good agreement with the full simulation; the results of Methods A and B with smaller cells are very close, the only appreciable difference being the frequency of the end mode. For the latter, Method A is in better agreement with the full simulation. The frequencies of the higher-order modes calculated with our methods show an appreciable dependence on the size of the mesh; high resolution is needed to obtain a reasonable agreement with the full simulation. Finally, we remark that the OOMMF results are within 0.5 GHz of the results of Method A.

The dynamical matrix approach provides, in addition to the modes in Table I, information on modes with oscillations in the direction perpendicular to the applied field. Such modes were not observed in Ref. 14, because of the type of perturbations used in that investigation. Two of these modes are shown in Fig. 1, one antisymmetric and the other symmetric with respect to a plane parallel to the applied field.

The frequency of these modes as a function of their wavevector is plotted in Fig. 2.

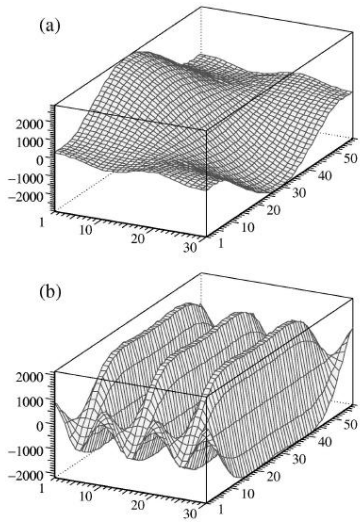


FIG. 1: Mode profiles of two DE-like modes; (a) 1-node mode with $\Omega = 58.6$ GHz, (b) 6-node mode with $\Omega = 138.2$ GHz. Method A with $58 \times 30$ cells. We plot the real part of $\delta m_z$ (arbitrary units) as a function of the cell position. As explained in the text, the imaginary part is zero.

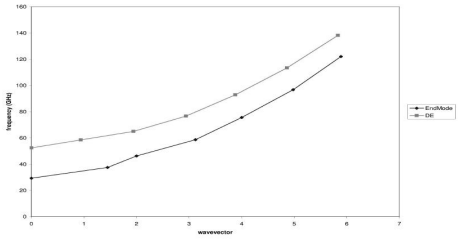


FIG. 2: Variation of the normal mode frequencies with the wavevector. The wavevector is perpendicular to $H$ and is plotted in units of $\pi/w$. Dots: DE-like modes; squares: end modes.

The wavevector $q$ was extracted from the distance between nodes or crests. The linear, increasing, dependence on $q$ at low frequencies is consistent with the expectation for DE-like modes. At larger $q$ however, instead of curving downwards as predicted by dipolar theory, the dispersion curves upwards. This effect can be traced to exchange interaction. It is worthy of note that, although all these modes appear to be unpinned (as judged by their amplitudes at the edges), the resulting wavevectors do not exactly correspond to the expected $n\pi/w$ with $n$ an integer and $w$ particle width ($w = 60$ nm).

We also observed a family of modes localized at the ends but with structure along the width. Both symmetric and antisymmetric modes with respect to a plane parallel to the applied field are found. As for the symmetric and antisymmetric end modes discussed in Ref. 14, each of these modes is actually a pair of almost degenerate modes, which are symmetric and antisymmetric with respect to a plane perpendicular to the applied field. A few of these modes are shown in Fig. 3.

The dispersion of these modes is also shown in Fig. 2. Although in this case we do not have any analytical theory with which to compare, the behavior of the two dispersions in Fig. 2 is similar, showing that the standing wave feature peperdicular to $H$ plays the same role in the two families of modes.

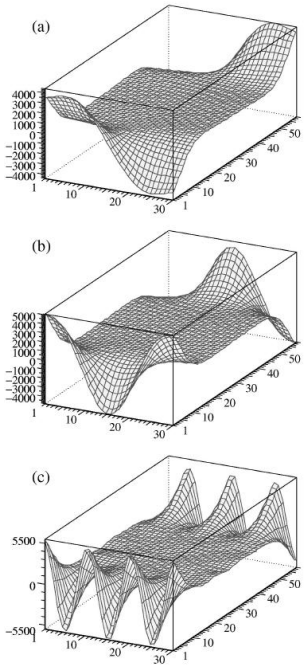


FIG. 3: Mode profiles of three end modes; (a) 1-node mode with $\Omega = 37.5$ GHz, (b) 2-node mode with $\Omega = 46.3$ GHz, (c) 6-node mode with $\Omega = 122.0$ GHz. See Fig. 1 for details.

The localization of modes at the ends of the particle is in agreement with the considerations presented in Ref. 12. According to these authors, the existence of localized modes is related to the strong inhomogeneity of the demagnetizing field along the length of the particle (that is, along the field direction), while the demagnetizing field is almost constant along the width of the particle. The above inhomogeneity leads to DE-like standing waves (Fig. 1) extending in the central region where the demagnetizing field is almost constant and quite small, and also to modes at the end regions where the demagnetizing field is large but also quite homogeneous. It is interesting to note that sum of two complementary modes profiles, for example those plotted in Fig. 1(b) and Fig. 3(c), gives rise to an ideal standing wave insensitive to the lateral confinement. Consistent with the absence of large inhomogeneities in the demagnetizing field along the particle width, we have not found any edge-modes localized at the sides of the sample.

In addition, we also find a large variety of two-dimensional modes with nodes along both directions, like the $9 \times 2$ mode reported in Ref. 14 and listed in Table I. These types of modes are expected in the simple "standing wave" picture. However, because the standing wave picture is too simplistic, these modes can show hybridization effects. Figure 4 shows the profile of the two modes at 64.6 and 66.1 GHz.

The sum and difference of the two eigenvectors, shown in Fig. 5, are the modes that would be predicted in the standing wave approximation.

In our finite particle, these two modes hybridize to yield the profiles shown in Fig. 4.

## IV. CONCLUSIONS

We have shown that a dynamical matrix approach yields the correct frequencies and profiles of the normal modes of a magnetized particle. The approach requires considerably less computational power than the micromagnetic approach where the time dependence of each spin in the system is tracked.[14] However, contrary to the micromagnetic approach, the dynamical matrix approach does not allow for probing nonlinear effects, nor does it yield information regarding which modes are excited in pulsed field experiments.

For comparison purposes, we have applied the dynamical matrix approach to the particle studied with the micromagnetic approach in Ref. 14 — a $116 \times 60 \times 20$ nm Fe rectangular parallelepiped. We found the modes to be in

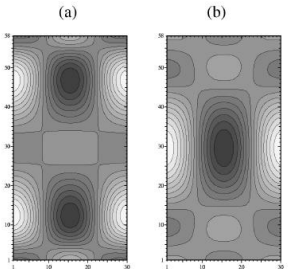


FIG. 4: Contour plot of two mode profiles of mixed character; (a) $\Omega = 66.1$ GHz, (b) $\Omega = 64.6$ GHz. Method A with $58 \times 30$ cells. We plot the real part of $\delta m_z$ (arbitrary units) as a function of the cell position.

excellent agreement. We also presented information on modes with wavevectors perpendicular to the applied field. In addition to the expected Daman-Eshback-like modes located in the center of the particle, we observed a family of similar modes localized at the sample ends.

The dynamical matrix approach allows the investigation of mode hybridization. Our results show the existence of modes which, if combined, yield plane wave-like solutions but which, due to the confined geometry, loose their plane-wave attributes.

### Acknowledgments

Work at the University of Ferrara supported by Ministerio Istruzione, Universita e Ricerca, grant PRIN 2003025857. Work at Argonne National Laboratory supported by the U.S. Department of Energy under Contract W-31-109-ENG-38. We thank R. Stamps and R. Zivieri for useful discussions.

## APPENDIX A: EQUATIONS OF MOTION

The equations of motion for a magnetic dipole in terms of the second derivatives of the total energy $H$ of the system can be derived from the first of the Hamilton equations,

$$\frac{\partial q_n}{\partial t} = \frac{\partial H}{\partial p_n}, \qquad \frac{\partial p_n}{\partial t} = -\frac{\partial H}{\partial q_n},$$

where the $q_n$ are the generalized variables of the problem and the $p_n$ the corresponding conjugate momenta. The direction of the magnetic dipole of the $k$th cell, which has a uniform magnetization, is given by Eq. (2). In this case, the dynamical variables are the small deviations from eqilibrium of its polar angles,

$$q_1 = \delta\phi_k, \qquad q_2 = \delta\theta_k.$$

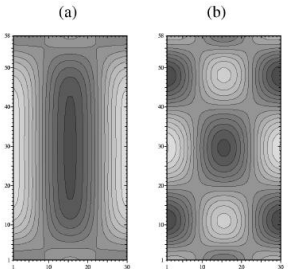


FIG. 5: Contour plot of two mode profiles derived from those in Fig. 4 as (a) sum and (b) difference, as described in the text.

The corresponding variation of angular momenta can be found recalling that a magnetic dipole of momentum $\boldsymbol{\mu}$ has an angular momentum $\boldsymbol{l} = \frac{1}{\gamma}\boldsymbol{\mu}$, where $\gamma$ is the gyromagnetic ratio. Therefore,

$$\boldsymbol{l} = \frac{1}{\gamma}\boldsymbol{\mu} = \frac{vM_s}{\gamma}\boldsymbol{m},$$

where $v$ is the volume of the cell. Since $q_1$ is a rotation of the magnetic dipole around the $z$ axis, its conjugate momentum $p_1$ corresponds to the $z$ component of the variation of angular momentum,

$$p_1 = \delta l_z = \frac{vM_s}{\gamma}\delta m_z = -\frac{vM_s}{\gamma}\sin\theta_k\,\delta\theta_k. \tag{A1}$$

The other momentum $p_2$ can be calculated analogously; $q_2$ is a rotation of the dipole moment around an axis (of unitary vector $\widehat{\boldsymbol{\phi}}' = -(\sin\phi)\hat{\boldsymbol{x}} + (\cos\phi)\hat{\boldsymbol{y}}$) in the $(x, y)$-plane, at an angle $\phi' = \phi + \pi/2$ from the $x$-axis. Therefore, $p_2$ corresponds to the projection on the $\widehat{\boldsymbol{\phi}}'$ vector of the variation of the angular momentum,

$$p_2 = \delta\boldsymbol{l}\cdot\widehat{\boldsymbol{\phi}}' = \frac{vM_s}{\gamma}\left(\frac{\partial\boldsymbol{m}}{\partial\phi}\delta\phi + \frac{\partial\boldsymbol{m}}{\partial\theta}\delta\theta\right)\cdot\widehat{\boldsymbol{\phi}}' = \frac{vM_s}{\gamma}\sin\theta_k\,\delta\phi_k. \tag{A2}$$

Using Eqs. (A1) and (A2) in the first Hamilton equation, we obtain the following system:

$$\begin{cases} \dfrac{\partial\,\delta\phi_k}{\partial t} = -\dfrac{\gamma}{vM_s\sin\theta_k}H_{\delta\theta_k}, \\ \dfrac{\partial\,\delta\theta_k}{\partial t} = \dfrac{\gamma}{vM_s\sin\theta_k}H_{\delta\phi_k}. \end{cases}$$

The first derivatives of the energy can be calculated by introducing the energy density $E = H/v$ and expanding it in power series, retaining only the leading terms,

$$E = \frac{1}{2}\sum_{n=1}^{N}\sum_{j=1}^{N}\left(E_{\phi_n\phi_j}\,\delta\phi_n\,\delta\phi_j + 2E_{\phi_n\theta_j}\,\delta\phi_n\,\delta\theta_j + E_{\theta_n\theta_j}\,\delta\theta_n\,\delta\theta_j\right),$$

where the derivatives must be calculated at equilibrium. Here, we have taken into account the vanishing of the first derivatives at equilibrium and neglected the inessential constant term. Thus we obtain the equations

$$\begin{cases} \dfrac{\partial\,\delta\phi_k}{\partial t} = -\dfrac{\gamma}{M_s \sin\theta_k} \displaystyle\sum_{j=1}^{N} \left( E_{\theta_k \phi_j}\,\delta\phi_j + E_{\theta_k \theta_j}\,\delta\theta_j \right), \\ \dfrac{\partial\,\delta\theta_k}{\partial t} = \dfrac{\gamma}{M_s \sin\theta_k} \displaystyle\sum_{j=1}^{N} \left( E_{\phi_k \phi_j}\,\delta\phi_j + E_{\phi_k \theta_j}\,\delta\theta_j \right). \end{cases}$$

By introducing the time dependence of the variable as $e^{i\Omega t}$ and rearranging some terms, we obtain Eq. (3).

## APPENDIX B: SECOND DERIVATIVES OF THE ENERGY DENSITY

The second derivative of the Zeeman energy is

$$E_{\alpha_k \beta_j} = \begin{cases} -M_s \boldsymbol{H} \cdot \dfrac{\partial^2 \boldsymbol{m}_k}{\partial\alpha_k \partial\beta_k} & k = j, \\ 0 & k \neq j. \end{cases}$$

The second derivative of the exchange energy is

$$E_{\alpha_k \beta_j} = \begin{cases} -\dfrac{2A}{d^2} \displaystyle\sum_{n=1}^{4} \dfrac{\partial^2 \boldsymbol{m}_k}{\partial\alpha_k \partial\beta_k} \cdot \boldsymbol{m}_n & k = j, \\ -\dfrac{2A}{d^2} \dfrac{\partial \boldsymbol{m}_k}{\partial\alpha_k} \cdot \dfrac{\partial \boldsymbol{m}_j}{\partial\beta_j} & k \text{ and } j \text{ nearest neighbors}, \\ 0 & k \text{ and } j \text{ far away}. \end{cases}$$

The second derivative of the dipolar energy is calculated by taking into account that the symmetric demagnetizing tensor satisfies the symmetry condition $\overleftrightarrow{N}(k,j) = \overleftrightarrow{N}(j,k)$. The result is

$$E_{\alpha_k \beta_j} = \begin{cases} M_s^2 \left( \displaystyle\sum_{\substack{n=1 \\ n \neq k}}^{N} \boldsymbol{m}_n \cdot \overleftrightarrow{N}(n,k) \dfrac{\partial^2 \boldsymbol{m}_k}{\partial\alpha_k \partial\beta_k} + \dfrac{\partial \boldsymbol{m}_k}{\partial\alpha_k} \cdot \overleftrightarrow{N}(k,k) \dfrac{\partial \boldsymbol{m}_k}{\partial\beta_k} \right. & \\ \left. \qquad + \boldsymbol{m}_k \cdot \overleftrightarrow{N}(k,k) \dfrac{\partial^2 \boldsymbol{m}_k}{\partial\beta_k \partial\alpha_k} \right) & k = j, \\ M_s^2 \dfrac{\partial \boldsymbol{m}_k}{\partial\alpha_k} \cdot \overleftrightarrow{N}(k,j) \dfrac{\partial \boldsymbol{m}_j}{\partial\beta_j} & k \neq j. \end{cases}$$

The second and third term inside the parenthesis in the expression for $k = j$ correspond to the self-interaction.

The partial derivatives of the magnetization which appear in the equations of this appendix are easily obtained from Eq. (2) and evaluated at equilibrium.

---


* Electronic address: grimsditch@anl.gov; URL: http://www.msd.anl.gov/groups/mf/index.html
† Electronic address: leaf@mcs.anl.gov; URL: http://www.mcs.anl.gov/~leaf
‡ Electronic address: kaper@mcs.anl.gov; URL: http://www.mcs.anl.gov/~kaper



[1] L. R. Walker, Phys. Rev. **105**, 390 (1957).
[2] L. R. Walker, J. Appl. Phys. **29**, 318 (1958).
[3] K. Yu. Guslienko and A. N. Slavin, J. Appl. Phys. **87**, 6337 (2000).
[4] B. A. Ivanov and C. E.Zaspel, Appl. Phys. Lett. **81**, 1261 (2002).
[5] V. Novosad, M. Grimsditch, K. Yu. Guslienko, P. Vavassori, Y. Otani, and S. D. Bader, Phys. Rev. B **66**, 052407 (2002).
[6] OOMMF User's Guide, Version 1.0, M. Donahue and D. Porter. Interagency report NISTIR 6376. National Institute of Standards and Technology, Gaithersburg, MD.
[7] R. Hertel and J. Kirschner, ICM Conference, Rome 2003 and J. Magn. Magn. Mater., to be published.

[8] D. R. Fredkin and T. R. Koehler, IEEE Trans. Magn. **26**, 415 (1990).
[9] Y. Roussigné, S. M. Chérif, and P. Moch, J. Mag. Mag. Mat. **263**, 289 (2003).
[10] J. Jorzick, S. O. Demokritov, B. Hillebrands D. Berkov, N. L. Gorn, K. Yu. Guslienko, and A. N. Slavin, Phys. Rev. Lett. **88**, 047204 (2002).
[11] J. P. Park, P. Eames, D. M. Engebretson, J. Berezovsky and P. A. Crowell, Phys. Rev. Lett. 89, 277201 (2002).
[12] K. Yu. Guslienko, R. W. Chantrell, and A. N. Slavin, Phys. Rev. B **68**, 024422 (2003).
[13] C. Bayer, S. O. Demokritov, B. Hillebrands, and A. N. Slavin, Appl. Phys. Lett. **82**, 607 (2003).
[14] M. Grimsditch, G. K. Leaf, H. G. Kaper, D. A. Karpeev, and R. E. Camley, Phys. Rev. B, submitted.
[15] M. Grimsditch, S. Kumar, and E. E. Fullerton, Phys. Rev. B **54**, 3385 (1996).
[16] R. Zivieri, L. Giovannini and F. Nizzoli, Phys. Rev. B **62**, 14950 (2000).
[17] J. Smit and H. G. Beljers, Philips Res. Rep. **10**, 113 (1955).
[18] Z. Zhang, L. Zhou, P. E. Wigen, and K. Ounadjela, Phys. Rev. B **50**, 6094 (1994).
[19] A. J. Newell, W. Williams, and D. J. Dunlop, J. Geoph. Res. **98**, 9551 (1993).
[20] M. E. Schabes and A. Aharoni, IEEE Trans. Magn. MAG-23, 3882 (1987).
[21] J. D. Jackson, *Classical Electrodynamics*, (John Wiley & Sons, New York, 1975).